

Article

**Dispersive Kinetics from Single Molecules Oriented  
in Single Crystals of Potassium Acid Phthalate**

Kristin L. Wustholz, Eric D. Bott, Christine M. Isborn, Xiaosong Li, Bart Kahr, and Philip J. Reid

*J. Phys. Chem. C*, **2007**, 111 (26), 9146-9156 • DOI: 10.1021/jp0713559

Downloaded from <http://pubs.acs.org> on January 23, 2009

**More About This Article**

Additional resources and features associated with this article are available within the HTML version:

- Supporting Information
- Links to the 5 articles that cite this article, as of the time of this article download
- Access to high resolution figures
- Links to articles and content related to this article
- Copyright permission to reproduce figures and/or text from this article

[View the Full Text HTML](#)

## Dispersive Kinetics from Single Molecules Oriented in Single Crystals of Potassium Acid Phthalate

Kristin L. Wustholz, Eric D. Bott, Christine M. Isborn, Xiaosong Li, Bart Kahr,\* and Philip J. Reid\*

Department of Chemistry, University of Washington, Box 351700, Seattle, Washington 98195-1700

Received: February 16, 2007; In Final Form: April 6, 2007

The intermittent emission or “blinking” of single violamine R (**1**) and 2',7'-dichlorofluorescein (**2**) molecules incorporated into single crystals of potassium acid phthalate (KAP) is studied using confocal fluorescence microscopy. Blinking dynamics are quantified in terms of switching rates and on- and off-length probability distributions. Mixed crystals of KAP/**1** and KAP/**2** consist of photophysical subpopulations with ~40% and ~20% exhibiting persistent emission, respectively, and the remainder demonstrating a broad range of blinking behavior that is well described by a power-law distribution. The dependence of the power-law exponent on chromophore, experimental bin time, intensity threshold, and excitation power is examined. The blinking dynamics are also modeled using Monte Carlo simulations on the basis of a three-level electronic system with the rate constants for population and depopulation of the “dark” state being distributed. No correlation between molecular orientation and blinking dynamics is observed, suggesting that intermolecular electron transfer is not the origin of power-law behavior. Alternative origins for this behavior (e.g., conformational flexibility and spectral diffusion) are explored using a combination of experimental and computational techniques. Of these possibilities, the distributed kinetics exhibited by KAP/**1** and KAP/**2** are attributed to spectral diffusion.

### Introduction

The emission from a single molecule under continuous photoexcitation is often intermittent, a phenomenon referred to as “blinking”. Typically, the observation of single-molecule blinking has been taken as evidence for molecules undergoing excursions to nonemissive states (e.g., a low-lying triplet state).<sup>1,2</sup> In this framework, the simple-exponential kinetics of dark-state population and depopulation are quantified by the variation in the temporal duration of emissive and nonemissive periods (i.e., on and off lengths).<sup>3</sup> However, many studies have observed broad distributions of on and off lengths that are inconsistent with single-exponential rate processes for dark-state population and decay.<sup>4–12</sup> Instead, the distribution of on and off times were found to demonstrate power-law behavior. Potential explanations for behavior have included molecular rotation,<sup>13</sup> conformational changes to a nonemissive state,<sup>6,9,14,15</sup> spectral diffusion,<sup>16–18</sup> reversible photooxidation,<sup>19,20</sup> and, more recently, intermolecular electron transfer.<sup>4,5,8,10,12</sup> For example, power-law blinking behavior of single molecules of rhodamine 6G on glass<sup>8</sup> and in poly(vinyl alcohol),<sup>12</sup> as well as Atto565 on glass,<sup>10</sup> have been attributed to the formation of nonemissive radicals through electron transfer between the emitter and the surroundings. The environmental heterogeneity characterizing these systems provides for a distribution of electron donor and acceptor distances and a corresponding distribution of electron-transfer rates. Although there is general agreement that blinking is an intrinsic characteristic of single-molecule emission, ambiguity persists regarding the nature of the dark state and the mechanism of dark-state population and depopulation for systems that demonstrate distributed kinetics.

Although numerous mechanisms for distributed blinking kinetics have been explored, many of these studies are complicated by the heterogeneous environment surrounding the molecule (e.g., solution, glass, polymer films). Single crystals, on the other hand, provide a unique environment in which to study single-molecule photophysics. The environment provided by a crystal lattice is ordered and restrictive, wherein translation and rotation are constrained by the host lattice. In addition, molecular bleaching due to photooxidation is reduced relative to oxygen-permeable matrices, and the decrease in nonradiative relaxation caused by the restrictive environment affords enhanced photostability.<sup>21</sup> Although traditional attempts to incorporate chromophores into host crystals have been limited to the regime where the host and guest are isomorphous,<sup>22,23</sup> we have demonstrated the use of potassium acid phthalate (KAP)<sup>21,24</sup> and K<sub>2</sub>SO<sub>4</sub><sup>25,26</sup> matrices to study a variety of organic dye molecules in the regime of nonisomorphous incorporation.

In this study, we investigate the photophysics of single molecules incorporated into single crystals of KAP (space group *Pca*2<sub>1</sub>, *a* = 9.614 Å, *b* = 13.330 Å, *c* = 6.479 Å)<sup>27</sup> that are formed as large {010} plates, with perfect cleavage parallel to these faces. KAP is easily grown from aqueous solution at room temperature in the presence of many luminophores. The resulting “dyed crystals”<sup>28</sup> can exhibit *inter-* and *intra*sectorally zoned molecular inclusions due to differences in affinity for colored molecules expressed by faces and vicinal surfaces of the crystal that are not related by symmetry. We previously characterized the alignments of single violamine R (**1**) molecules in KAP (Figure 1).<sup>29</sup> This dye solely recognizes the {010} growth sector of KAP (i.e., intersectoral zoning). Moreover, only the fast slopes of growth hillocks that are produced by the propagation of screw dislocations during crystal growth are dyed (i.e.,

\* Authors to whom correspondence should be addressed. E-mail: Bkahr@chem.washington.edu (B.K.); preid@chem.washington.edu (P.J.R.).

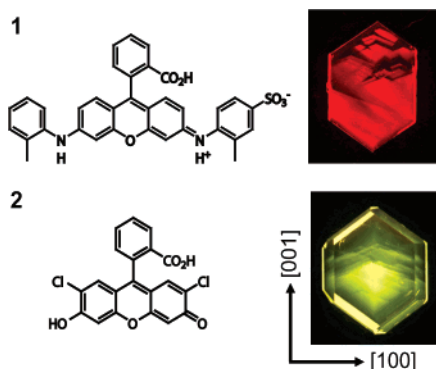


**Figure 1.** Dye-inclusion KAP crystals. Violamine R (**1**) and 2',7'-dichlorofluorescein (**2**) incorporate into the fast slopes of growth hillocks within the  $\{010\}$  growth sector of KAP, as evidenced by emission photographs.

intrasectoral zoning).<sup>29</sup> This work demonstrated the utility of mixed crystals with anisomorphous guests for single-molecule studies and provided the impetus to study molecular photo-physics in this well-defined environment. Herein, we investigate the blinking from individual molecules of **1** and 2',7'-dichlorofluorescein (**2**), a structural analog of **1** with reduced conformational flexibility (Figure 1), embedded in single KAP crystals. Confocal fluorescence microscopy is used to monitor the single-molecule-emission time traces that are subsequently quantified in terms of switching rates and on- and off-length probability distributions. The single-molecule blinking dynamics are modeled using Monte Carlo simulations involving a simple three-level electronic system. Finally, the mechanisms leading to blinking are explored by a combination of experimental and computational techniques. Overall, the study of single molecules in a single-crystal matrix provides novel insight into the origin and interpretation of blinking dynamics from organic fluorophores. Our results demonstrate that the dark-state population and decay kinetics of single molecules embedded in KAP are distributed. The observation of distributed kinetics for molecules incorporated in this well-defined environment suggests that electron transfer is not exclusively responsible for this behavior. Instead, we propose that power-law behavior of the blinking dynamics is attributed to changes in the interaction between the emitter and the surrounding dielectric leading to spectral diffusion.

## Experimental Section

Dye-inclusion crystals were grown as described previously.<sup>29</sup> **1** and **2** (Aldrich) were dissolved in deionized water (Barnstead NANOpure,  $18.2 \text{ M}\Omega \text{ cm}^{-1}$ ) or a small amount of ethanol, respectively, prior to addition to the aqueous crystal-growth solution (110 g/L of KAP). Heavily dyed crystals were grown from  $\sim 0.1 \text{ mM}$  dye solutions and characterized using polarized absorption microscopy (Olympus BX-50, Si-Photonics 440) and fluorescence spectroscopy (FluoroMax-2). Single crystals of KAP/**1** and KAP/**2** with chromophore densities suitable for single-molecule investigations were grown from  $\sim 5 \text{ nM}$  dye solutions. The segregation coefficient ( $\sigma_{\text{seg}}$ ), defined as the mole ratio of dye in the crystal to dye in the growth solution, was determined by absorbance measurements of redissolved crystals. For heavily dyed crystals of KAP/**1** and KAP/**2**,  $\sigma_{\text{seg}}$  is  $\sim 0.4\%$ , corresponding to approximately 1 dye molecule/10 000 KAP molecules in the  $\{010\}$  growth sector. Fluorescence lifetime measurements were performed using a commercial spectrophotometer (Photon Technology International) by employing 536-nm excitation and monitoring the emission centered at 600 nm

with a  $\sim 30\text{-nm}$  bandpass. Fluorescence lifetimes were determined by fitting the measured fluorescence decay to a single-exponential function convolved with the instrument response, with the latter measured using the scattering from a colloidal silica suspension (Aldrich, LUDOX AS-30). The best fit was determined through minimization of the reduced  $\chi^2$  statistic.

Single-molecule studies were performed using an inverted confocal microscope described in detail elsewhere.<sup>29</sup> Dyed crystals were mounted on a scan stage (Queensgate, NPS-XY-100B) and photoexcited at low power (3.5–6.4  $\mu\text{W}$ ) using a 532-nm Nd:YVO<sub>4</sub> (Spectra Physics, Millennia) or 405-nm solid-state diode (Photonic Products, PMMF108-4) laser. The excitation field was filtered (Chroma, Z532/10-nm bandpass for 532-nm excitation or D405/10-nm bandpass for 405-nm excitation), reflected toward the sample using an appropriate dichroic mirror (Chroma, Z532RDC or Z405RDC), and focused to a diffraction-limited spot using a  $100\times$  oil-immersion objective (Nikon, PlanFluor 1.3 NA). Epi-fluorescence was collected from the sample, passed through the dichroic mirror, spectrally filtered using an emission filter (Chroma, HQ550-nm long-pass for 532-nm excitation and HQ435-nm long-pass for 405-nm excitation), and spatially filtered with a confocal pinhole (CVI, 75- $\mu\text{m}$  diameter). Emission was detected using a single-photon-counting avalanche photodiode (Perkin-Elmer, SPCM-AQR-16). Total emission intensity following linearly polarized excitation modulated with a half-waveplate (CVI Laser) between the  $[100]$  and  $[001]$  crystal eigenmodes was measured over a  $10 \times 10 \mu\text{m}^2$  area by scanning the sample using a 100-nm step size and 100-ms integration time/point. Transition dipole moment orientations ( $\theta$ ) were computed according to  $\theta = \tan^{-1}(1.132DR)^{-1/2}$ , where the dichroic ratio ( $DR = I_a/I_c$ ) is corrected for sample birefringence.<sup>30</sup> Reported values of  $\theta$  are defined with respect to  $[100]$  in the  $ac$ -plane. Single-molecule-emission time traces were collected for 100 s, employing a 50-ms integration time per point. Data collection was accomplished using software constructed in-house using Labview (National Instruments). Geometry optimization and excited-state calculations were performed within the Gaussian03 program suite using the Pople 6-31G\* basis set.<sup>31</sup> Ground-state geometries were optimized using the B3LYP<sup>32,33</sup> functional, and excited-state properties were determined using the time-dependent Hartree Fock method.

Molecular transitions between emissive (“on”) and non-emissive (“off”) states, commonly referred to as blinking, were quantified as follows. First, an intensity threshold was defined to establish when the molecule exists in an emissive state. Setting the proper threshold is critical to accurately quantify blinking that occurs over multiple time scales since both fast and slow blinking can be obscured by setting a threshold that is artificially or carelessly assigned.<sup>34</sup> Single-molecule-emission time traces in KAP/**1** and KAP/**2** typically exhibit two emissive intensities consistent with “on” and “off” periods ( $I_{\text{on}}$  and  $I_{\text{off}}$ ), with the latter corresponding to a background intensity of  $\sim 20$  counts/50 ms. Threshold values corresponding to the average between the mean on and off intensities (i.e.,  $(\langle I_{\text{on}} \rangle + \langle I_{\text{off}} \rangle)/2$ ) were employed. The intensity at a given time above and below the threshold value was set to 1 and 0, respectively. A “switch” was defined as a transition from 1 to 0, or vice versa, with the switching rate corresponding to the number of switches/100 s. Since intensity was measured using a 50-ms integration time, the smallest measurable switching rate is  $0.05 \text{ s}^{-1}$ . On (off) lengths were defined as the temporal duration of successive on (off) events prior to a switch. To evaluate the impact of the threshold on the measured blinking dynamics, all data were evaluated with thresholds corresponding to 20% below and

above  $\langle I_{\text{on}} \rangle$  and  $\langle I_{\text{off}} \rangle$ , respectively. The on (off) length probability densities ( $P(\tau_{\text{on/off}})$ ) were computed by compiling histograms of the on (off) lengths for many molecules and dividing each value in the distribution by the average time to its nonzero nearest neighbors, consistent with the procedure outlined by Kuno and co-workers.<sup>35</sup> Single molecules that did not switch or switched just once as well as permanent off events corresponding to molecular photobleaching were not included in the analyses.

## Results and Discussion

Heavily dyed crystals of KAP/1 demonstrate a 544-nm absorption maximum and a 609-nm fluorescence maximum. The fluorescence lifetime ( $\tau_f$ ) of **1** in heavily dyed KAP is  $2.70 \pm 0.23$  ns, with the error corresponding to the standard deviation of the mean. This value is comparable to the solution-phase lifetimes for related fluorophores (e.g., 2.99 ns for rhodamine 110 in ethanol,<sup>36</sup> 4.08 ns for rhodamine 6G in ethanol,<sup>36</sup> and 2.17 ns for rhodamine B in methanol<sup>37</sup>). In contrast, in the crystal-growth solution the  $\tau_f$  of **1** ( $\lambda_{\text{max}} = 525$  nm,  $\lambda_{\text{em}} = 570$  nm) could not be resolved within the temporal response of the spectrophotometer ( $\sim 1$  ns). The enhancement in  $\tau_f$  for **1** in KAP compared to solution is consistent with a decrease in excited-state internal conversion due to the conformational restrictions provided by the host lattice, as reported for other dye-inclusion KAP crystals.<sup>21</sup>

The ensemble-averaged orientation of the absorption transition dipole moment of **1** in heavily dyed KAP/1 was determined by polarized absorption microscopy to be  $41.8 \pm 1.6^\circ$  from [100] in the *ac*-plane. Single-molecule measurements on KAP/1 established that the average orientation for 200 molecules was  $41.5 \pm 14.0^\circ$  (one standard deviation from the mean), in agreement with the bulk measurement. However, the distribution of orientations was substantial, with a fwhm (full-width half-maximum) of  $\sim 30^\circ$  and individual values ranging from  $8.1$  to  $74.1^\circ$  relative to [100]. Both the average orientation and distribution are in agreement with our previously reported results.<sup>29</sup>

**Blinking Dynamics in Violamine R (1)-Dyed KAP.** Given this distribution of individual molecular orientations, we sought to determine the range of photophysical behavior demonstrated by single molecules embedded in KAP. Figure 2 presents emission time traces of 3 representative single molecules. The molecule in Figure 2a demonstrates persistent emission for the duration of the experiment. In contrast, the molecule in Figure 2b exhibits frequent transitions between on and off states reminiscent of the blinking demonstrated by other molecular fluorophores<sup>3,38</sup> and semiconductor quantum dots.<sup>39</sup> The emission time trace shown in Figure 2c demonstrates substantially different blinking time scales, with two off events that last for more than 30 s. Similar behavior was reported for multichromophoric dendrimers dispersed in a polymer, where frequent blinking was observed with off events on the order of microseconds accompanied by infrequent off events that lasted hundreds of milliseconds.<sup>40</sup> Although the durations of these two off events in Figure 2c are much longer than typical triplet lifetimes,<sup>41</sup> triplet lifetimes of luminophores in mixed crystals can be significantly enhanced relative to solution due to conformational restrictions provided by the host, and phosphorescence lifetimes on the order of seconds to minutes have been observed.<sup>26,42</sup>

To characterize the diverse photophysics demonstrated by KAP/1, and to explore the nature of the nonemissive state, a quantitative analysis of the blinking dynamics was performed.

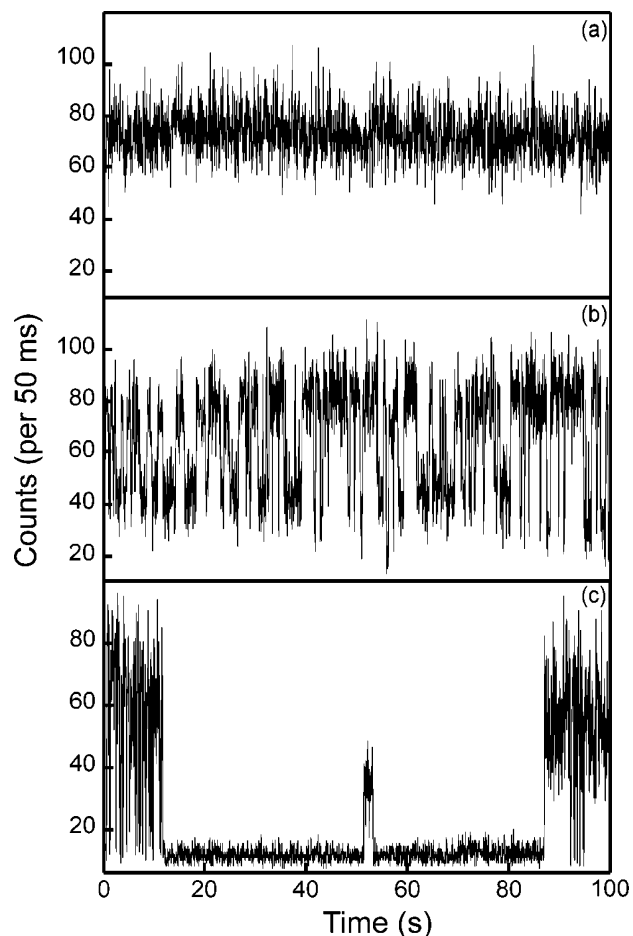


**Figure 2.** Emission time traces (100-s length and 50-ms integration time) of three representative single molecules of **1** embedded in KAP exhibiting (a) persistent emission, (b) periodic blinking, and (c) both fast and slow blinking (i.e., two off events lasting  $>30$  s).

Blinking dynamics in KAP/1 were quantified in terms of switching rates ( $\text{s}^{-1}$ ) and on- and off-length distributions. The distribution of switching rates for 205 molecules is presented in Figure 3a. The average switching rate was  $1.37 \pm 1.94 \text{ s}^{-1}$ , with the error representing one standard deviation from the mean. The distribution of switching rates can be approximated by a biexponential function with amplitudes ( $A$ ) and time constants ( $\tau$ ):  $A_1 = 101$ ,  $\tau_1 = 0.03$  s;  $A_2 = 4.2$ ,  $\tau_2 = 2.8$  s. Of 205 molecules, 79 (38.5%) exhibit persistent emission and are subsequently characterized as simply being “on”. For the remaining 126 molecules that demonstrate blinking, the distribution of switching rates (Figure 3a, inset) is substantial, ranging from  $0.05$  to  $8.38 \text{ s}^{-1}$ . The best fit of this subset of the total distribution to a biexponential function corresponds to  $A_1 = 480$ ,  $\tau_1 = 0.19$  s and  $A_2 = 4.4$ ,  $\tau_2 = 3.4$  s. In summary, these data suggest the presence of two subpopulations in the crystal, molecules that exhibit continual luminescence and the remainder that displays a broad distribution of blinking time scales.

What is the origin of the wide variation in photophysical behavior evident in Figure 3a? To address this question, we examined the connection between the orientational and photophysical heterogeneity demonstrated by KAP/1. Statistically improbable molecular orientations (i.e., values beyond one standard deviation from the mean) presumably originate from kinetic rather than thermodynamic factors governing crystal growth, and the photophysical behavior arising from a kinetically determined distribution of molecular orientations may differ significantly from that of a molecular distribution that share a

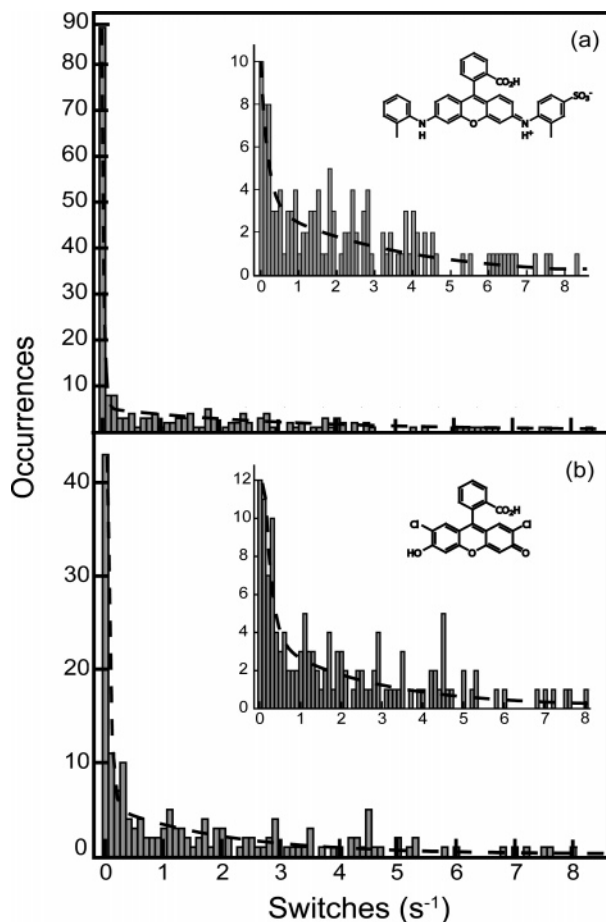


**Figure 3.** Distribution of switching rates ( $\text{s}^{-1}$ ) for (a) 205 molecules in KAP/1 and (b) 168 molecules in KAP/2. The average switching rates were found to be  $1.37 \pm 1.94$  and  $1.64 \pm 1.96 \text{ s}^{-1}$ , respectively. For KAP/1,  $\sim 40\%$  of the molecules are “on” (i.e., switching rate =  $0 \text{ s}^{-1}$ ), and the remainder (inset, a) demonstrate a wide variety of switching rates, corresponding to a biexponential fit (dashed line). For KAP/2,  $\sim 20\%$  of the molecules are “on” and the rest (inset, b) demonstrate biexponentially distributed switching rates.

stereochemical homology with the docking surface of the host. The relationship between photophysics and alignment was investigated by successive measurements of the emission and orientation of 93 molecules in KAP/1. The average orientation for this set of molecules was  $40.5 \pm 14.0^\circ$  from [100], demonstrating that the collection is representative of the overall alignment. In addition, the average switching rate was  $1.5 \text{ s}^{-1}$ , with values ranging from 0 to  $7.6 \text{ s}^{-1}$ , demonstrating that a representative distribution of photophysical behavior was also observed. Plots of the switching rate with respect to orientation are shown in Figure 4a, and no correlation between orientation and photophysical behavior is observed.

To further characterize the blinking dynamics of single molecules in KAP/1, the temporal duration of emissive and nonemissive events were compiled into on- and off-length histograms. Since an individual molecule demonstrates a limited number of on and off events, data from 40 single molecules were combined to perform this analysis consistent with recent work by Yeow and workers,<sup>10</sup> with the corresponding histograms containing 4269 emissive events and 4271 nonemissive events presented in Figures 5a and 6a, respectively. Figure 5a demonstrates that on lengths range from 0.05 s (the experimental resolution) to 98.8 s. The corresponding off-length distribution consists of events ranging from 0.05 to 76.0 s. Both the on- and off-length distributions are peaked at short times, with the

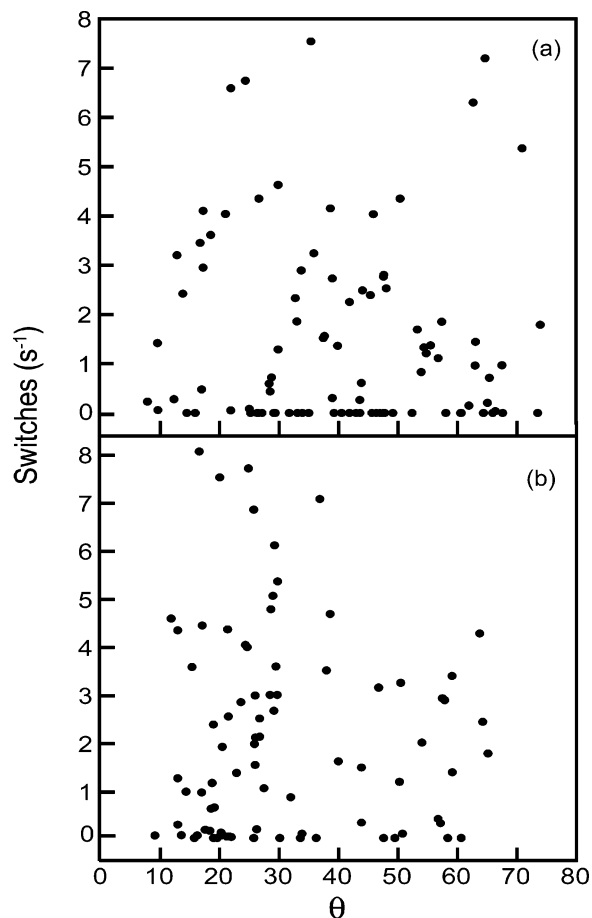


**Figure 4.** Scatter plots of the switching rates ( $\text{s}^{-1}$ ) and orientations of (a) 93 molecules in KAP/1 and (b) 82 molecules in KAP/2. No correlation between photophysics and alignment is observed.

number of extremely long events ( $>30 \text{ s}$ ) being limited. Consistent with previous analyses, continuous distributions of the on- and off-length probability densities ( $P(\tau_{\text{on/off}})$ ) were derived from these data by dividing each value in the on- (off-) length distribution by the average time to its nonzero nearest neighbors.<sup>35</sup> The resulting semilogarithmic plots of  $P(\tau_{\text{on}})$  and  $P(\tau_{\text{off}})$  are shown in Figures 5b and 6b, respectively. An initial attempt to describe the probability densities using a biexponential function produced best-fit values for  $P(\tau_{\text{on}})$  of  $A_1 = 4686 \text{ s}^{-1}$ ,  $\tau_1 = 0.53 \text{ s}$  and  $A_2 = 20 \text{ s}^{-1}$ ,  $\tau_2 = 10.4 \text{ s}$  (Figure 5b) and for  $P(\tau_{\text{off}})$  of  $A_1 = 2697 \text{ s}^{-1}$ ,  $\tau_1 = 0.49 \text{ s}$  and  $A_2 = 21 \text{ s}^{-1}$ ,  $\tau_2 = 8.0 \text{ s}$  (Figure 6b). However, comparison of the data to the fit reveals that the biexponential functions do not adequately describe the experimental distributions. Instead, both  $P(\tau_{\text{on}})$  and  $P(\tau_{\text{off}})$  are well described employing a power-law expression of the form  $P(\tau_{\text{on/off}}) = P_0 \tau_{\text{on/off}}^{-m_{\text{on/off}}}$  where  $m_{\text{on/off}}$  is the power law exponent. Plots of  $P(\tau_{\text{on}})$  and  $P(\tau_{\text{off}})$  and the best fits to the power-law function corresponding to  $P_0(\text{on}) = 371$ ,  $m_{\text{on}} = 2.0$  and  $P_0(\text{off}) = 208$ ,  $m_{\text{off}} = 1.8$  are presented in Figures 5c and 6c, respectively. For comparison, the power-law exponents observed for other systems are  $m \sim 1.7$  for semiconductor nanocrystals,<sup>35,43,44</sup>  $m \sim 2$  for single molecules on glass,<sup>8,10</sup> and  $m \sim 1.4$  for molecules dispersed in polymers.<sup>4,5</sup> To investigate the impact of the threshold value (used to define when the molecule exists in an emissive or nonemissive state) on the on- and off-length distributions, data analyses were repeated using threshold intensities corresponding to 20% below and above  $\langle I_{\text{on}} \rangle$  and  $\langle I_{\text{off}} \rangle$ , respectively. The resulting on- and off-length distributions exhibited power-law dependence with slightly modified exponents of  $m_{\text{on}} = 1.7, 1.7$  and  $m_{\text{off}} = 1.8, 2.0$ . These

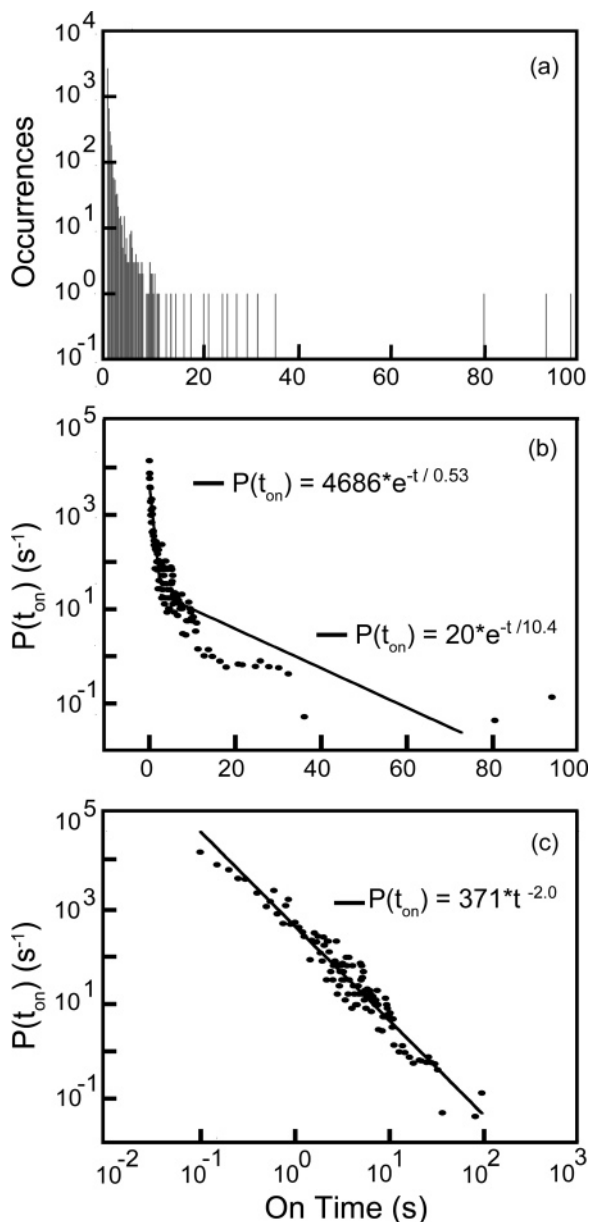


**Figure 5.** On-length probability distribution for 40 single molecules in KAP/I: (a) on-length distribution comprised of 4269 emissive events that range from 0.05 to 98.8 s; (b) semilogarithmic plot of the resulting probability density ( $P(\tau_{\text{on}})$ ) fit with a biexponential function (solid lines) that does not sufficiently represent the data; (c)  $P(\tau_{\text{on}})$  presented on a logarithmic scale, with a power-law fit to the data (solid line) corresponding to  $m_{\text{on}} = 2.0$ .

data demonstrate that power-law behavior is persistent and provides a measure of the uncertainty in the power-law exponent ( $\sim 0.3$ ) originating from threshold selection.

The expectation value for the average time in the on or off state ( $\langle\tau_{\text{on/off}}\rangle$ ) was obtained from the best fit to the power-law distribution according to  $\langle\tau\rangle = [(m - 1)/(m - 2)]\tau_{\text{max}}^{(2-m)}\tau_{\text{min}}^{(m-1)}$ .<sup>35,45</sup> From the power-law fits for KAP/I, where  $\tau_{\text{max}}$  is the longest on (off) length and  $\tau_{\text{min}}$  is the integration time of the experiment (50 ms), values of  $\langle\tau_{\text{on}}\rangle = 0.38$  s and  $\langle\tau_{\text{off}}\rangle = 0.74$  s were obtained. Emission time traces for 24 molecules obtained using a 10-ms bin time were compiled to give >10 000 emissive and nonemissive events yielding power-law fits corresponding to  $m_{\text{on}} = 2.3$ ,  $m_{\text{off}} = 2.0$ ,  $\langle\tau_{\text{on}}\rangle = 0.03$  s, and  $\langle\tau_{\text{off}}\rangle = 0.10$  s, demonstrating the dependence of the average on and off times on the experimental integration time as well as the insensitivity of  $m$  to this perturbation.

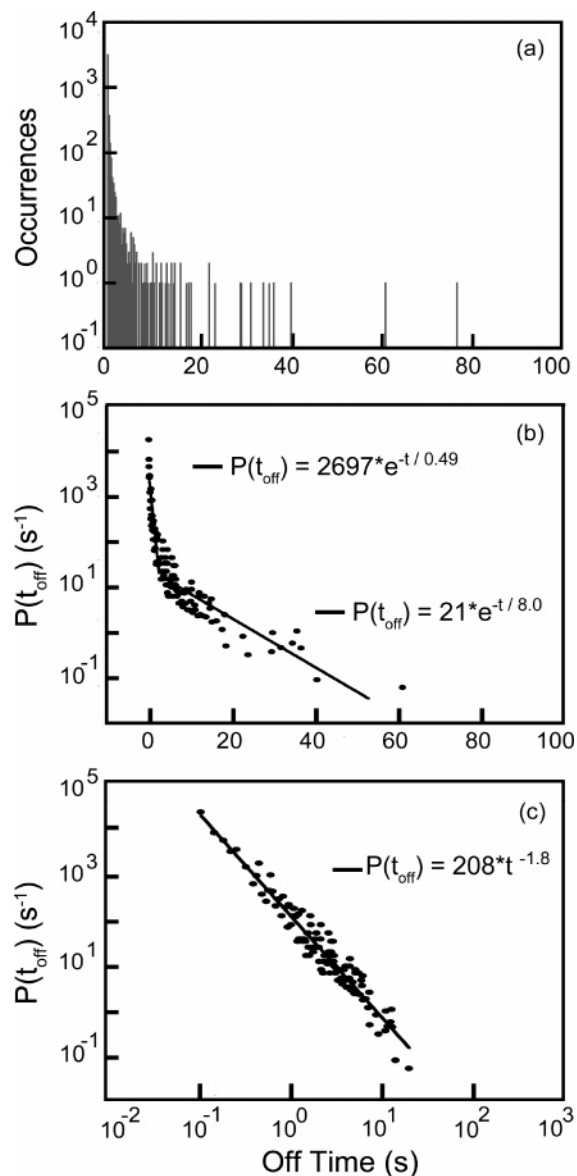


**Figure 6.** Off-length probability distribution for 40 single molecules in KAP/I: (a) distribution comprised of 4271 nonemissive events ranges from 0.05 to 76.0 s; (b) semilogarithmic plot of  $P(\tau_{\text{off}})$  presented with a biexponential fit (solid lines) that does not represent the data; (c) logarithmic plot of  $P(\tau_{\text{off}})$ , with a power-law fit (solid line) corresponding to  $m_{\text{off}} = 1.8$ .

#### Power-Law Blinking Behavior in Individual Molecules.

Studies of emission intermittency from semiconductor quantum dots have found power-law behavior for individual quantum dots, consistent with statistics derived from collections of dots.<sup>46</sup> Since the power-law behavior observed for the collection of molecules in KAP/I shown in Figures 5 and 6 could arise from the averaging over many molecules with distributed single-exponential blinking rates, it is important to establish that individual chromophores also demonstrate power-law blinking behavior. Toward this end,  $P(\tau_{\text{on}})$  and  $P(\tau_{\text{off}})$  were calculated for *individual molecules* monitored for 1 h, with the observation of emission for the duration of these long-time measurements highlighting the stability that is provided by incorporation into the KAP lattice. All single molecules that exhibited blinking for >1000 s (long enough to provide sufficient statistics) produced power-law distributions, with  $\langle m_{\text{on}} \rangle = 1.8 \pm 0.4$  and  $\langle m_{\text{off}} \rangle = 1.4 \pm 0.2$ . Figure 7 presents the probability distributions for a representative molecule in KAP/I monitored for 1 h,

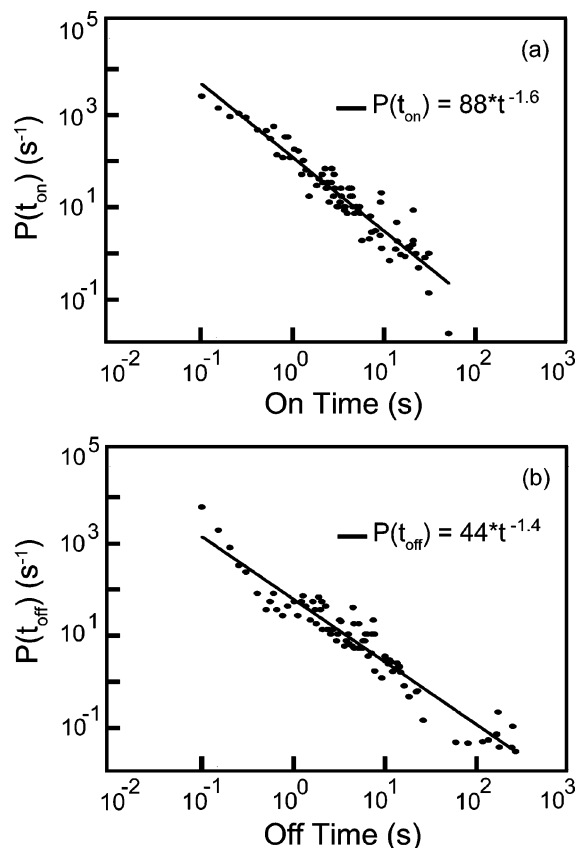


**Figure 7.** Logarithmic plots of the probability distributions of on lengths (a) and off lengths (b) for an individual molecule in KAP/1, with power-law fits (solid lines) corresponding to  $m_{\text{on}} = 1.6$  (least-squares fitting), 2.5 (MLE) and  $m_{\text{off}} = 1.4$  (least-squares fitting), 2.3 (MLE).

yielding 1645 emissive and 1270 nonemissive events. On and off lengths ranged from the resolution limit (0.05 s) to 169.2 and 322.2 s, respectively. The distributions for this molecule demonstrated power-law dependence with  $P_0(\text{on}) = 88$ ,  $m_{\text{on}} = 1.6$ , and  $\langle \tau_{\text{on}} \rangle = 1.7$  s and  $P_0(\text{off}) = 44$ ,  $m_{\text{off}} = 1.4$ , and  $\langle \tau_{\text{off}} \rangle = 8.3$  s. Recently, a maximum likelihood estimator (MLE) method for analyzing power-law distributed data with particular application to limited datasets (i.e., individual emitters) has been described.<sup>47</sup> Applying the MLE method to the total dataset consisting of 40 molecules of KAP/1 resulted in power-law exponents of  $m_{\text{on}} = 1.8$  and  $m_{\text{off}} = 2.2$ . For the molecule in Figure 7, the MLE method produced values of  $m_{\text{on}} = 2.5$  and  $m_{\text{off}} = 2.3$ , indicating that the power-law exponents for the molecule are closer to the values obtained from analysis of the composite blinking statistics. Overall, these results demonstrate that power-law dependence of the blinking dynamics is observed for individual molecules, suggesting that the power-law distribution for the collection of 40 molecules does not arise from averaging of dispersive single-exponential rates for individual molecules (i.e., static) but rather reflects dynamically changing rate constants for dark-state population and depopulation.<sup>10,35,45,48</sup> It should be noted that power-law behavior from single perylene trimers on glass and in PMMA has been observed, consistent with the behavior determined through the analysis of blinking statistics for collections of these molecules.<sup>5</sup>

**Monte Carlo Simulations.** Previous authors have used Monte Carlo (MC) simulations based on an electron-tunneling model to reproduce the distributed kinetics observed in blinking studies of semiconductor quantum dots<sup>45,49</sup> and for molecular fluorophores.<sup>10</sup> The distributed kinetics of single molecules have been

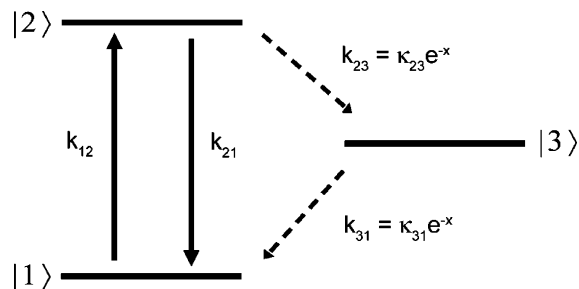


**Figure 8.** Physical model employed in the MC simulations. Three electronic levels considered correspond to the singlet ground state ( $|1\rangle$ ), the singlet excited state ( $|2\rangle$ ), and a “dark” state ( $|3\rangle$ ). The photoexcitation and emission rate constants are fixed on the basis of experimental conditions (solid arrows), while the dark-state population ( $k_{23}$ ) and depopulation ( $k_{31}$ ) rate constants are distributed (dashed arrows).

modeled by MC simulations employing a four-level system wherein tunneling to the dark state occurs via a long-lived triplet state.<sup>10</sup> Interestingly, the results of these simulations were unchanged upon removal of the triplet state, suggesting that a simpler three-level system is sufficient to successfully reproduce the distributed kinetics that give rise to power-law blinking dynamics. Accordingly, we performed MC simulations of blinking dynamics employing a model with three electronic levels: the singlet ground state ( $|1\rangle$ ), the singlet excited state ( $|2\rangle$ ), and a “dark” state ( $|3\rangle$ ) (Figure 8). The photoexcitation rate constant ( $k_{12}$ ) is restricted to  $1 \times 10^6 \text{ s}^{-1}$  on the basis of the experimental laser power and absorption cross section of **1**. The radiative rate constant ( $k_{21}$ ) is fixed at  $3.7 \times 10^8 \text{ s}^{-1}$  consistent with the measured fluorescence lifetime of KAP/1. To account for power-law behavior, the dark-state population ( $k_{23}$ ) and depopulation ( $k_{31}$ ) rate constants were modeled as follows:

$$k_{ij} = \kappa_{ij} e^{-x}$$

In the above expression,  $i$  and  $j$  are the initial and final states, respectively,  $\kappa_{ij}$  is the preexponential factor, and  $x$  is a random number generated from an exponential distribution.<sup>45</sup>

Single-molecule population trajectories were simulated through iterative comparison of a uniformly distributed random number to the probability of leaving the occupied electronic state according to

$$P_{|i\rangle} = 1 - e^{-\sum_j k_{ij} t}$$

In this expression,  $t$  is the computational time step (1 ns). Since  $k_{ij} t \ll 1$ , the probability can be approximated as  $P_{|i\rangle} = \sum_j k_{ij} t$ . If the molecule resides in the ground state, only the probability of excitation is tested. Similarly, if the molecule populates the dark state only the probability of relaxation to the ground state is tested. The situation is more complex if the molecule populates the singlet excited-state since population transfer can occur via  $|2\rangle \rightarrow |1\rangle$  or  $|2\rangle \rightarrow |3\rangle$ . To determine which of these pathways is taken, the simulation first tests if depopulation from  $|2\rangle$  will happen, on the basis of comparison of  $P_{|2\rangle} = k_{21}t + k_{23}t$  to a random number. If depopulation occurs, the  $|2\rangle \rightarrow |1\rangle$  emissive pathway is tested on the basis of the fluorescence quantum yield,  $\Phi_f = k_{21}/(k_{21} + k_{23})$ . If emission happens, a count is added to the large (50 ms) time bin. Otherwise, a transition to the dark state occurs. To model the blinking dynamics for the mixed crystals,  $\kappa_{23}$  and  $\kappa_{31}$  were adjusted until the experimental fluorescence trajectories, power-law exponents, and  $\langle \tau_{\text{on/off}} \rangle$  were reproduced. Once obtained, the simulated fluorescence time traces were analyzed in the same manner as

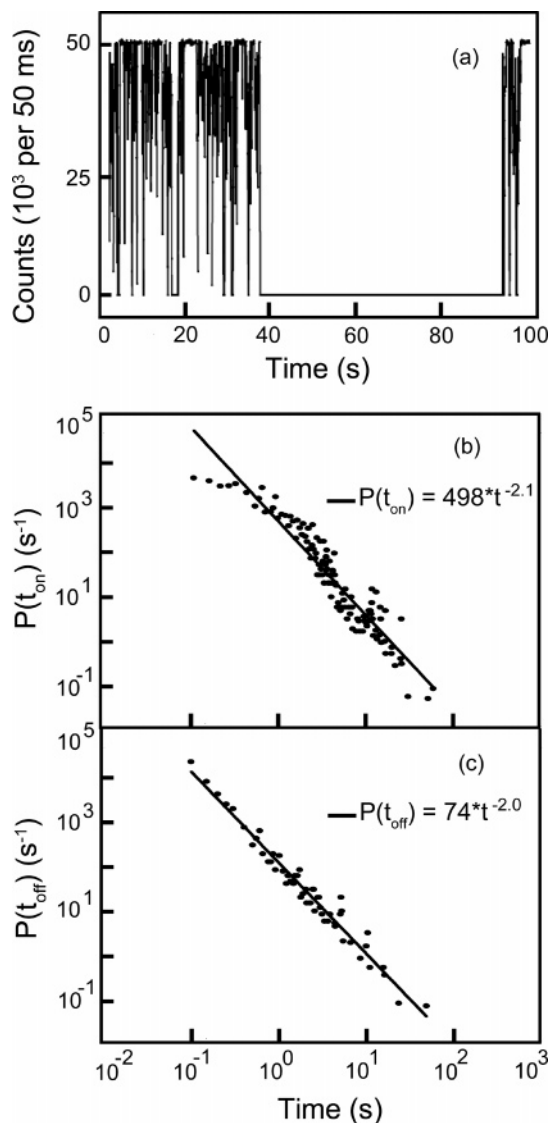


**Figure 9.** Results of MC simulations: (a) representative simulated emission time trace employing a 50-ms bin, 1-ns computational time step, and  $k_{12} = 10^6 \text{ s}^{-1}$ ,  $k_{21} = 3.7 \times 10^8 \text{ s}^{-1}$ ,  $\kappa_{23} = 10^6 \text{ s}^{-1}$ , and  $\kappa_{31} = 10^4 \text{ s}^{-1}$ . The resulting on- and off-length probability distributions from 40 simulated traces and corresponding power-law fits are shown in (b)  $m_{\text{on}} = 2.1$  and (c)  $m_{\text{off}} = 2.0$ , respectively.

the experimentally obtained traces to determine the probability distributions  $P(\tau_{\text{on/off}})$ .

To model blinking dynamics in KAP/1, 40 simulations were performed with  $\kappa_{23}$  and  $\kappa_{31}$  set to  $10^6$  and  $10^4 \text{ s}^{-1}$ , respectively. Figure 9a presents a simulated 100-s emission time trace employing a 50-ms bin time and the corresponding probability densities determined using a threshold of the average between on and off intensities. On lengths ranging from 0.05 to 60.9 s were observed in the simulations, as well as off lengths ranging from 0.05 to 57.8 s. The probability distributions of on- and off-length durations from the simulated data are presented in Figure 9b,c, respectively. The best fit corresponded to power-law expressions with  $P_0(\text{on}) = 498$ ,  $m_{\text{on}} = 2.1$ , and  $\langle \tau_{\text{on}} \rangle = 0.30$  and  $P_0(\text{off}) = 74$ ,  $m_{\text{off}} = 2.0$ , and  $\langle \tau_{\text{off}} \rangle = 0.34$  s, in good agreement with the experimental distributions. It should also be noted that the simulations predicted average switching rates consistent with the experimental rates for the subset of molecules that exhibited blinking. Previous MC simulations of single Atto565 molecules immobilized on glass produced power-law exponents of  $m_{\text{on}} = 2.8$  and  $m_{\text{off}} = 2.0$ , using  $\kappa_{23}$  and  $\kappa_{31}$  values

of  $4 \times 10^9$  and  $10^6 \text{ s}^{-1}$ .<sup>10</sup> For MC simulations of quantum-dot blinking, previous authors obtained  $m_{\text{on}} = 2.2$  and  $m_{\text{off}} = 2.0$ , using  $\kappa_{23}$  and  $\kappa_{31}$  values of  $10^7$  and  $10^5 \text{ s}^{-1}$ .<sup>45</sup> Comparison of these results to our simulated data demonstrates the relative insensitivity of the power-law exponent to the preexponential factors. Blinking studies of **1** in polymer matrices are underway to explore the variation in the microscopic rate constants predicted by the MC simulations. Furthermore, experimental studies of **1** in KAP using a 10-ms bin time revealed that the power-law exponent is relatively insensitive to changes in the experimental bin time. Overall, these results demonstrate that the  $m$  value is not particularly informative and suggest that the power-law exponent in combination with the average on and off times ( $\langle \tau_{\text{on/off}} \rangle$ ) provides a more useful description of blinking behavior.

The current and previous MC simulations<sup>10,45</sup> are based on a model that incorporates two distributed-kinetic processes. For completeness, we also considered the case where either population or depopulation of the dark state is distributed. This study was motivated by the possibility that while the transition to the dark state may be distributed, the dark-state decay rate could be constant, and vice versa. When population transfer to the dark state was distributed, the resulting on-length probability density was fit by a power-law expression with  $m_{\text{on}} = 1.8$ , but the off-length probability density was well modeled with a single-exponential function with  $\tau_{\text{off}} = 1.04$  s. Conversely, when population transfer to the dark state was assigned to a fixed rate but the dark-state lifetimes were distributed,  $P(\tau_{\text{on}})$  and  $P(\tau_{\text{off}})$  revealed single exponential and power-law character, respectively. These results demonstrate that, for both  $P(\tau_{\text{on}})$  and  $P(\tau_{\text{off}})$  to follow power-law behavior, pathways to and from the dark state must be distributed.

**Origin of Distributed Kinetics.** The origin of distributed kinetics has been a recent topic of interest. For example, the population kinetics of long-lived dark states in semiconductor quantum dots have been extensively studied and are proposed to originate from distributed electron-transfer kinetics.<sup>35,43,45,48–51</sup> Perhaps more relevant to the system of interest here, the power-law distributions of emissive and nonemissive times for single molecules of rhodamine 6G in poly(vinyl alcohol)<sup>12</sup> and on glass,<sup>8</sup> as well as Atto565 on glass,<sup>10</sup> have been assigned to the formation of nonemissive radicals produced by populating the long-lived triplet state, followed by electron tunneling. In this model, nonemissive radicals are thought to form through electron transfer between the molecule and its surroundings, with the distribution of transfer rates arising from the disordered arrangement of the “solvent”. Support for this hypothesis was provided by Zondervan et al., who measured the ESR spectrum of a photoexcited polymer film containing single molecules of rhodamine 6G and observed a transition consistent with radical formation.<sup>12</sup>

In contrast to the aforementioned studies, distributed kinetics are observed here for molecules incorporated in a rigid, ordered, and well-defined crystalline environment. This observation is both informative and confounding with respect to the electron-transfer hypothesis that relies on the disordered nature of the surrounding matrix to explain the origin of the distributed kinetics. Furthermore, if charge transfer were occurring in the crystal, one would expect a correlation between molecular orientation and blinking dynamics consistent with the orientational- and distance-dependence of electron transfer. However, no correlation between molecular orientation and blinking was observed (Figure 4a). Given the issues surrounding assignment of the distributed kinetics for KAP/1 to intermolecular electron

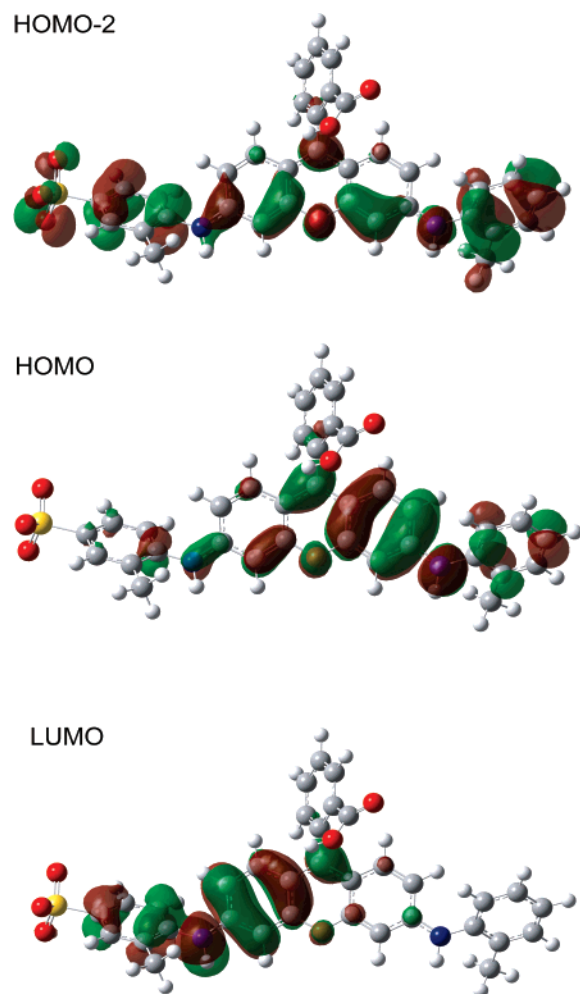


**Figure 10.** HF/6-31G\* molecular orbitals of **1**. The lowest energy excited state is dominated by transitions from the HOMO-2 and HOMO to LUMO, corresponding to an energy of 616 nm and oscillator strength of 0.84. Electron density is predominately localized along the xanthenone backbone and terminal rings of **1**.

transfer, other origins for power-law dependence of the blinking dynamics were explored.

**Conformational Flexibility and Blinking Behavior.** Extended dark periods in single-molecule emission studies have also been attributed to time- and environment-dependent conformational changes of molecules<sup>9</sup> such as the formation of twisted intramolecular charge transfer (TICT) conformers.<sup>15</sup> In the case of **1**, it is possible that variation in blinking behavior reflects a distribution of conformational flexibility provided by various crystal nanoenvironments. To explore this hypothesis, linear-response time-dependent Hartree Fock calculations (TD-HF) were performed to determine the conformational dependence of the excited-state properties of **1**.<sup>52</sup> TD-HF/6-31G\* calculations on the optimized ground-state geometry of **1** predicted a visible transition at 616 nm with significant oscillator strength (0.84) that is dominated by the transitions from the HOMO-2 and HOMO to the LUMO (Figure 10). In the HOMO-2 and HOMO, electron density is localized along the xanthenone backbone and terminal aryl rings of the chromophore and is shifted to the xanthenone backbone and sulfonated ring upon excitation to the LUMO. These results suggest that rotation about the terminal rings of **1** may alter the molecular orbital overlap, thereby affecting the oscillator strength and/or the absorption and emission energies.

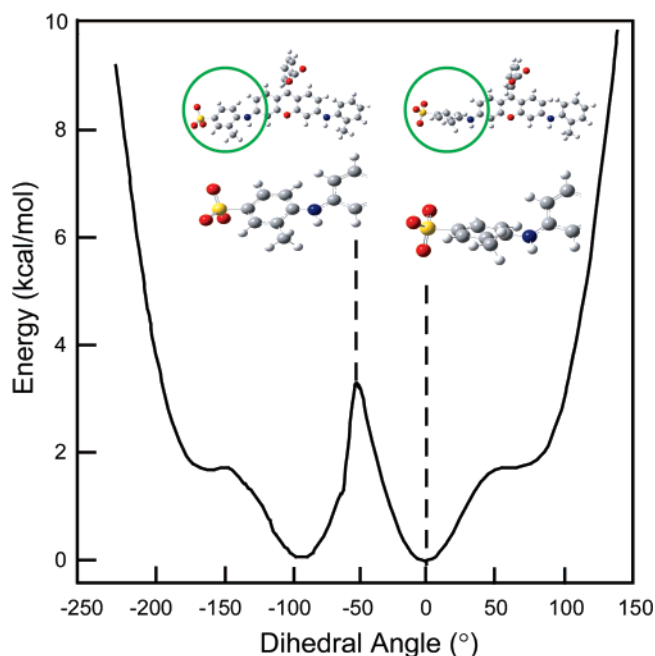


**Figure 11.** B3LYP/6-31G\* ground-state potential energy surface of **1**. Energies corresponding to rotation of the sulfonated ring around the single bond connecting it to the xanthenone backbone of **1** (circled) are presented, where 0° corresponds to the dihedral angle for the lowest energy conformer. Energy maxima due to hydrogen/hydrogen (~4 kcal/mol) and methyl/hydrogen (~10 kcal/mol) steric interactions as well as minima at dihedral angles of -160, -86, and 75° are demonstrated.

To determine the number and accessibility of low-energy molecular conformers, the ground-state potential energy surface (PES) along the single-bond torsional coordinate for the bond connecting the sulfonated ring to the xanthenone backbone was determined (Figure 11). For reference, 0° is associated with the lowest energy ground-state geometry of **1**. The activation barrier for rotation to the molecular conformer with hydrogen/hydrogen steric hindrance is 4 kcal/mol (~1400 cm<sup>-1</sup>), and that for methyl/hydrogen sterics is 10 kcal/mol (~3000 cm<sup>-1</sup>). According to these results, several molecular conformations corresponding to dihedral angles of -160, -86, and 75° may be thermally accessible at room temperature. TD-HF/6-31G\* calculations predicted that the energy and oscillator strength of the lowest energy transition for the conformer at -86° are not modified relative to the ground-state geometry. However, at the shallow minima corresponding to dihedral angles of -160 and 75°, the terminal aryl rings of **1** are completely out of conjugation with the xanthenone backbone. As a result, the lowest energy excitation is predicted to shift to ~1000 nm. These results suggest that spectral diffusion, caused by time- or environment-dependent conformational changes around the sulfonated ring of **1**, is responsible for the variation in blinking behavior. Yet, the “dark conformations” exist at relatively shallow energy minima, casting doubt on the conformational origin for long-lived dark states. It should be noted the PES of **1** could be significantly modified in the crystal and various molecular conformers might be stabilized by the surrounding dielectric environment.

To further explore the role of conformational flexibility in the distributed kinetics of **1**, we performed experiments on 2',7'-dichlorofluorescein (**2**) incorporated into KAP (Figure 1). This chromophore is structurally analogous to **1** but lacks the sulfonated phenyl ring such that this potential source for conformational dependence of the transition dipole moment is eliminated. Ensemble-averaged and single-molecule experiments

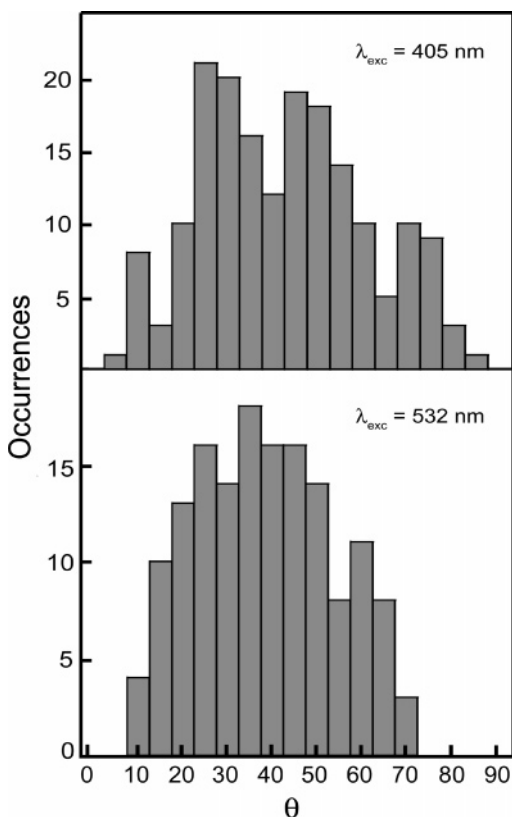


**Figure 12.** Orientational distributions (NA 1.3, bin size = 5°) of **2** in KAP. Top: Histogram of orientations for 180 molecules employing 405-nm excitation, measured as an angle between 0 and 90° from [100]. The average was found to be  $42.4 \pm 18.3^\circ$  from [100]. Bottom: Orientations of 151 molecules excited at 532 nm, with the average corresponding to  $38.3 \pm 15.4^\circ$  from [100]. The fwhm of the orientational distributions following 405- and 532-nm excitation are  $\sim 55$  and  $\sim 50^\circ$ , respectively.

on KAP/2 were performed. Heavily dyed crystals of KAP/2 exhibit absorption maxima at 475 and 502 nm, corresponding to a mixture of the neutral (20.7%), monoanionic (66.3%), and dianionic (13.1%) species<sup>53,54</sup> consistent with the fractional composition of the crystal-growth solution at a pH of 4.5. Following 502-nm illumination, the crystal exhibits a fluorescence maximum at 531 nm with a shoulder at 570 nm. The average orientation of the absorption dipole moment of **2** in the fast slopes of growth hillocks in the {010} sector of KAP as determined by absorption anisotropy was  $51.4 \pm 2.2^\circ$  from [100] in the *ac*-plane. For single-molecule experiments employing 405-nm excitation, the average orientation of 180 molecules in KAP/2 was found to be  $42.4 \pm 18.3^\circ$  from [100], with values ranging from 5.7 to 86.5° (Figure 12). The single-molecule measurements were repeated using 532-nm excitation to rule out photoselection. With 532-nm excitation, the average orientation for 151 molecules in KAP/2 was found to be  $38.3 \pm 15.4^\circ$  from [100], with the orientational distribution ranging from 9.2 to 70.7° (Figure 12). The fwhm of the orientational distributions following 405- and 532-nm excitation were  $\sim 55$  and  $\sim 50^\circ$ , respectively. These results demonstrate that single molecules are poorly aligned in the crystal host, despite the fact that heavily dyed crystals demonstrate specific chemical zoning that directs dyes to the fast slopes of growth hillocks. The persistent difference between the average orientation from bulk and single-molecule measurements in KAP/2 is presumably a consequence of hillock habit modification in the presence of high dye concentrations. This phenomenon is under investigation.

The photophysics of **2** were quantified as described previously. First, the switching rates ( $s^{-1}$ ) (the rate of switching between emissive and nonemissive states/100-s time trace) were determined using 532-nm excitation, with the switching rates for 168 molecules of **2** presented in Figure 3b. The average switching rate was  $1.64 \pm 1.96 s^{-1}$ . Of the sampled molecules, 31 (18.5%) exhibit persistent emission and are “on”. The blinking dynamics of the remaining 137 molecules, shown in the inset of Figure 3b, extend over a wide range of switching rates, with values ranging from 0.05 to 8.04  $s^{-1}$ . The distribution of switching rates observed for KAP/2 is remarkably similar to that observed for KAP/1 and again suggests the existence of two photophysical subpopulations in the crystal. The relationship between photophysics and chromophore alignment was investigated by successive measurements of emission and molecular orientation of 82 fluorophores in KAP/2, with plots of the switching rate with respect to orientation shown in Figure 4b. The average orientation was determined to be  $31.2^\circ$  from [100], and the average switching rate was  $2.1 s^{-1}$ , with values ranging from 0 to 8.04  $s^{-1}$ . Finally, Figure 4b demonstrates no obvious correlation between absorption dipole moment orientation and blinking dynamics, reminiscent of the case for KAP/1.

To determine the influence of chromophore architecture on blinking, on- and off-length histograms were compiled from the emission time traces of 72 single molecules of **2**. From these molecules, histograms containing 4481 emissive events and 4473 nonemissive events were obtained that include on and off lengths from the limit of resolution (0.05 s) to 63.9 and 49.7 s, respectively. The changes in  $P(\tau_{\text{on}})$  and  $P(\tau_{\text{off}})$  with time were initially fit to a sum of two exponentials. The best fit of a biexponential function to  $P(\tau_{\text{on}})$  corresponds to  $A_1 = 4759 s^{-1}$ ,  $\tau_1 = 0.47 s$  and  $A_2 = 33.5 s^{-1}$ ,  $\tau_2 = 6.5 s$  and for  $P(\tau_{\text{off}})$  to  $A_1 = 4520 s^{-1}$ ,  $\tau_1 = 0.45 s$  and  $A_2 = 29.5 s^{-1}$ ,  $\tau_2 = 8.3 s$ . Similar to the case of KAP/1, these functions did not accurately reproduce the observed distributions. Figure 13a,b demonstrates that power-law behavior is observed for KAP/2, with best fit to the power-law expression corresponding to  $P_0(\text{on}) = 308$ ,  $m_{\text{on}} = 1.9$ , and  $\langle \tau_{\text{on}} \rangle = 0.44$  and  $P_0(\text{off}) = 284$ ,  $m_{\text{off}} = 1.7$ , and  $\langle \tau_{\text{off}} \rangle = 0.76 s$ . The power dependence of the on- and off-length distributions was explored by increasing the laser excitation power by a factor of 1.5, and the resulting on- and off-length histograms and power-law exponents remained unchanged. Overall, our results demonstrate that power-law behavior is observed for single molecules in both KAP/2 and KAP/1, and this similarity suggests that the distributed kinetics for KAP/1 are not associated with conformational flexibility.

**Dielectric Environment and Blinking Behavior.** Environmental heterogeneity may be responsible for the distributed kinetics demonstrated by **1** and **2**. Although the KAP lattice is fixed, periodic, and ordered, it is likely that single molecules experience a variety of nanoenvironments within the crystal. Specifically, the variety of incorporation geometries that were measured supports the idea that the first coordination sphere of an embedded dye, defined as the spherical volume that encompasses its nearest crystalline neighbors, is variable. In these subvolumes, differences in the proximity and orientation of phthalate and potassium ions relative to the dye molecule will impact its dielectric environment and, subsequently, the excited-state energies. Therefore, modest relaxation of the surrounding dielectric environment around a fixed dye molecule could lead to spectral diffusion over time. In addition, KAP acts as an acidic buffer ( $pK_a = 4.2$ ) such that the anionic forms of the chromophores (where the carboxylic acid is deprotonated) are certainly present in the mixed crystals in addition to the

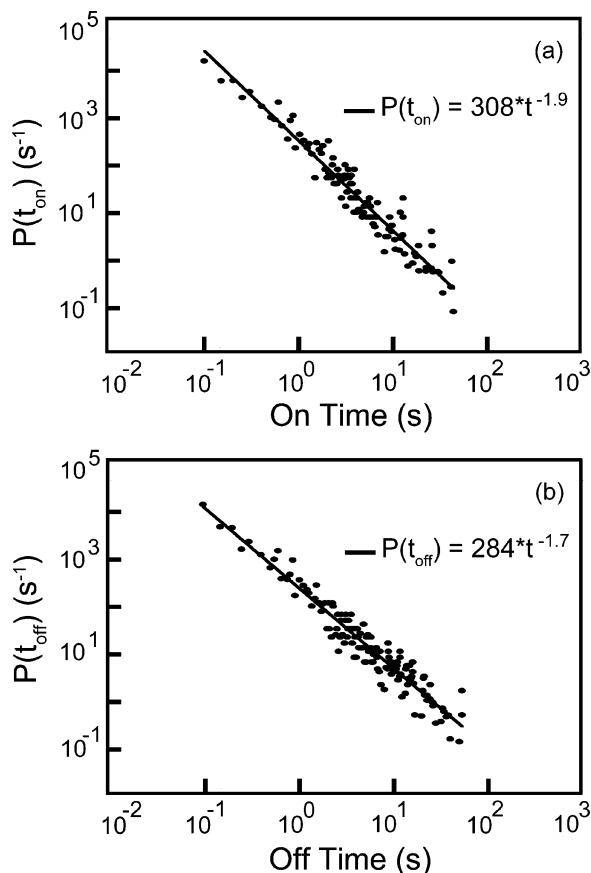


**Figure 13.** Logarithmic plots of the probability distributions of on lengths (a) and off lengths (b) for 72 molecules in KAP/2, with power-law fits (solid lines) corresponding to  $m_{\text{on}} = 1.9$  and  $m_{\text{off}} = 1.7$ , respectively.

zwitterionic form of **1** and the neutral and dibasic forms of **2**, which introduces the possibility of photoinduced formation of their nonfluorescent lactone forms.<sup>55,56</sup>

To explore the influence of the surrounding dielectric on molecular energetics, preliminary linear-response time-dependent density functional theory (TD-DFT) calculations were performed on the anionic form of **1** in the presence of a potassium cation. TD-DFT/6-31G\* results demonstrate that when the cation is close to the carboxylate or sulfonate moiety of the anionic dye, the visible absorption spectrum is hypsochromatically shifted up to  $\sim 100$  nm relative to the chromophore alone, suggesting that spectral diffusion is responsible for changes in emission intensity.<sup>16,17</sup> Furthermore, the excited states of the anionic dye contain more electron density on the carboxylate group, which significantly impacts the orbital overlap and energies of nearly all the transitions. These results support the role of nanoscale heterogeneity of the surrounding dielectric leading to spectral diffusion that is manifested as distributed blinking kinetics. Ultimately, these calculations highlight the importance of measuring the single-molecule energies, and this work is underway.

## Conclusion

Single-molecule microscopy was used to measure the alignment and photophysics of individual fluorophores incorporated into single crystals of KAP. Despite the specific chemical zoning present in heavily dyed mixed crystals, a wide variety of single-molecule orientations were observed, with orientational ranges that span  $66.0^\circ$  for KAP/1,  $61.5^\circ$  for 532-nm excitation of KAP/2, and  $80.8^\circ$  for 405-nm excitation of KAP/2. The blinking

dynamics of individual fluorophores were measured and quantified in terms of switches ( $\text{s}^{-1}$ ) and on- and off-length probability densities. Mixed crystals of KAP/1 and KAP/2 contained photophysical subpopulations of which  $\sim 40\%$  and  $\sim 20\%$  exhibited persistent fluorescence, respectively, and the remainder demonstrating a broad range of photophysical behavior. No correlations between molecular orientation and blinking dynamics were observed. Of the molecules that demonstrated blinking, on- and off-length histograms were compiled to yield power-law distributions where  $m \sim 2$ . Power-law behavior was also observed for *individual molecules* in KAP/1, suggesting that averaging of single-exponential behavior is not responsible for distributed kinetics. Monte Carlo simulations involving a three-level electronic system with distributed rate constants for dark-state population and depopulation were used to reproduce the experimental emission observed in KAP/1 and KAP/2. Rate constants corresponding to  $k_{12} = 10^6 \text{ s}^{-1}$ ,  $k_{21} = 3.7 \times 10^8 \text{ s}^{-1}$ ,  $\kappa_{23} = 10^6 \text{ s}^{-1}$ , and  $\kappa_{31} = 10^4 \text{ s}^{-1}$  yielded best fits to a power-law expression corresponding to  $P_0(\text{on}) = 498$ ,  $m_{\text{on}} = 2.1$ , and  $\langle \tau_{\text{on}} \rangle = 0.30$  and  $P_0(\text{off}) = 74$ ,  $m_{\text{off}} = 2.0$ , and  $\langle \tau_{\text{off}} \rangle = 0.34$  s, in reasonable agreement with the measured distributions.

Given the ordered nature of the KAP “solvent” and the fact that no correlations between molecular orientation and blinking were observed, intermolecular electron transfer is unlikely to be solely responsible for the distributed kinetics demonstrated by KAP/1 and KAP/2. Therefore, other causes of distributed blinking kinetics were explored. First, TD-HF was used to explore the likelihood that conformational changes about the sulfonated ring of **1** will occur and subsequently modify the excitation energy and/or oscillator strength of the lowest energy transition. Computations provided evidence that more than one molecular conformation is accessible at room temperature, and conformationally induced spectral diffusion may lead to the variation in blinking behavior. However, experiments on KAP/2 (with **2** lacking the terminal aryl rings in **1**) provided evidence that conformational flexibility is not responsible for distributed kinetics.

Relative to glass surfaces and polymer films, the KAP lattice provides a uniquely well-defined and ordered environment in which to study single molecules. However, the broad orientational distributions of **1** and **2** in KAP provided evidence that the first-coordination spheres of embedded dyes are surprisingly diverse, despite the specific chemical zoning that is observed in heavily dyed crystals. This nanoscale environmental heterogeneity and time-dependent relaxation of the surrounding dielectric are proposed to give rise to distributed kinetics for single molecules in KAP. Preliminary TD-DFT calculations on the anionic form of **1**, the principal species in the crystal-growth solution, predict that the visible absorption is hypsochromatically shifted up to 100 nm when a potassium cation was introduced near its sulfonate or carboxylate moiety. Since distributed kinetics were observed for an individual molecule, a dynamically changing property must be responsible for blinking behavior. Accordingly, two possible mechanisms for distributed kinetics are proposed: (1) time-dependent geometrical changes in the first-coordination sphere of a fixed molecule (i.e., dynamical spectral diffusion); (2) dynamic environmental and/or conformational heterogeneity in combination with a charge separation and recombination mechanism that occurs via exponentially varying population and depopulation rates. To explore these ideas, single-molecule emission and lifetime measurements as well as bulk time-resolved EPR experiments are underway. Furthermore, the environmental dependence of power-law behavior is under investigation through comparative studies of

1 in poly(methyl acrylate) and KAP.<sup>57</sup> The work presented here demonstrates that distributed kinetics are not limited to single molecules in disordered polymer and glass matrices but exist even for molecules incorporated in a single crystal. Moreover, these results motivate continued studies of single molecules in well-defined crystal hosts to establish the details of the blinking mechanism.

**Acknowledgment.** We thank the National Science Foundation for the generous support of this work through the Center on Materials and Devices for Information Technology Research (DMR-0120967). K.L.W. is a NSF-IGERT and University Initiative Funded fellow, supported by the Center for Nanotechnology at the University of Washington (Grant DGE-0504573). B.K. acknowledges NSF Grant CHE-0349882. We thank Ken Kuno (University of Notre Dame) and J. Michael Schurr (University of Washington) for helpful discussions about Monte Carlo simulations.

## References and Notes

- Basche, T.; Kummer, S.; Brauchle, C. *Nature* **1995**, *373*, 132.
- Kohn, F. H. J.; Gronheid, R.; Van der Auweraer, M.; De Schryver, F. C. *J. Phys. Chem. A* **2002**, *106*, 4808.
- Veerman, J. A.; Garcia-Parajo, M. F.; Kuipers, L.; van Hulst, N. F. *Phys. Rev. Lett.* **1999**, *83*, 2155.
- Haase, M.; Hubner, C. G.; Reuther, E.; Herrmann, A.; Mullen, K.; Basche, T. *J. Phys. Chem. B* **2004**, *108*, 10445.
- Hoogenboom, J. P.; van Dijk, E.; Hernando, J.; van Hulst, N. F.; Garcia-Parajo, M. F. *Phys. Rev. Lett.* **2005**, *95*, 097401.
- Osad'ko, I. S. *J. Exp. Theor. Phys.* **2003**, *96*, 617.
- Schuster, J.; Cichos, F.; von Borczyskowski, C. *Appl. Phys. Lett.* **2005**, *87*.
- Schuster, J.; Cichos, F.; von Borczyskowski, C. *Opt. Spectrosc.* **2005**, *98*, 712.
- Weston, K. D.; Buratto, S. K. *J. Phys. Chem. A* **1998**, *102*, 3635.
- Yeow, E. K. L.; Melnikov, S. M.; Bell, T. D. M.; De Schryver, F. C.; Hofkens, J. *J. Phys. Chem. A* **2006**, *110*, 1726.
- Yip, W. T.; Hu, D. H.; Yu, J.; Vanden Bout, D. A.; Barbara, P. F. *J. Phys. Chem. A* **1998**, *102*, 7564.
- Zondervan, R.; Kulzer, F.; Orlinskii, S. B.; Orrit, M. *J. Phys. Chem. A* **2003**, *107*, 6770.
- Ambrose, W. P.; Goodwin, P. M.; Martin, J. C.; Keller, R. A. *Phys. Rev. Lett.* **1994**, *72*, 160.
- Hofkens, J.; Vosch, T.; Maus, M.; Kohn, F.; Cotlet, M.; Weil, T.; Herrmann, A.; Mullen, K.; De Schryver, F. C. *Chem. Phys. Lett.* **2001**, *333*, 255.
- Hou, Y. W.; Higgins, D. A. *J. Phys. Chem. B* **2002**, *106*, 10306.
- Stracke, F.; Blum, C.; Becker, S.; Mullen, K.; Meixner, A. *J. Chem. Phys. Chem.* **2005**, *6*, 1242.
- Lu, H. P.; Xie, X. S. *Nature* **1997**, *385*, 143.
- Ambrose, W. P.; Basche, T.; Moerner, W. E. *J. Chem. Phys.* **1991**, *95*, 7150.
- Christ, T.; Kulzer, F.; Bordat, P.; Basche, T. *Angew. Chem., Int. Ed.* **2001**, *40*, 4192.
- Yu, J.; Hu, D. H.; Barbara, P. F. *Science* **2000**, *289*, 1327.
- Benedict, J. R.; Wallace, P. M.; Reid, P. J.; Jang, S. H.; Kahr, B. *Adv. Mater.* **2003**, *15*, 1068.
- Guttler, F.; Croci, M.; Renn, A.; Wild, U. P. *Chem. Phys.* **1996**, *211*, 421.
- Walla, P. J.; Jelezko, F.; Tamarat, P.; Lounis, B.; Orrit, M. *Chem. Phys.* **1998**, *233*, 117.
- Barbon, A.; Bellinazzi, M.; Benedict, J. B.; Brustolon, M.; Fleming, S. D.; Jang, S. H.; Kahr, B.; Rohl, A. L. *Angew. Chem., Int. Ed.* **2004**, *43*, 5328.
- Rifani, M.; Yin, Y. Y.; Elliott, D. S.; Jay, M. J.; Jang, S. H.; Kelley, M. P.; Bastin, L. D.; Kahr, B. *J. Am. Chem. Soc.* **1995**, *117*, 7572.
- Gurney, R. W.; Mitchell, C. A.; Ham, S.; Bastin, L. D.; Kahr, B. *J. Phys. Chem. B* **2000**, *104*, 878.
- Okaya, Y. *Acta Crystallogr.* **1965**, *19*, 879.
- Kahr, B.; Gurney, R. W. *Chem. Rev.* **2001**, *101*, 893.
- Wustholz, K. L.; Kahr, B.; Reid, P. J. *J. Phys. Chem. B* **2005**, *109*, 16357.
- Michl, J. T., E. W. *Spectroscopy with Polarized Light: Solute Alignment by Photoselection, in Liquid Crystals, Polymers, and Membranes*, 2nd ed.; VCH: New York, 1995.
- Frisch, M. J.; Trucks, G. W.; Schlegel, H. B.; Scuseria, G. E.; Robb, M. A.; Cheeseman, J. R.; Montgomery, J. A.; Vreven, J. T.; Kudin, K. N.; Burant, J. C.; Millam, J. M.; Iyengar, S. S.; Tomasi, J.; Barone, V.; Mennucci, B.; Cossi, M.; Scalmani, G.; Rega, N.; Petersson, G. A.; Nakatsuji, H.; Hada, M.; Ehara, M.; Toyota, K.; Fukuda, R.; Hasegawa, J.; Ishida, M.; Nakajima, T.; Honda, Y.; Kitao, O.; Nakai, H.; Klene, M.; Li, X.; Knox, J. E.; Hratchian, H. P.; Cross, J. B.; Bakken, V.; Adamo, C.; Jaramillo, J.; Gomperts, R.; Stratmann, R. E.; Yazyev, O.; Austin, A. J.; Cammi, R.; Pomelli, C.; Ochterski, J. W.; Ayala, P. Y.; Morokuma, K.; Voth, G. A.; Salvador, P.; Dannenberg, J. J.; Zakrzewski, V. G.; Dapprich, S.; Daniels, A. D.; Strain, M. C.; Farkas, O.; Malick, D. K.; Rabuck, A. D.; Raghavachari, K.; Foresman, J. B.; Ortiz, J. V.; Cui, Q.; Baboul, A. G.; Clifford, S.; Cioslowski, J.; Stefanov, B. B.; Liu, G.; Liashenko, A.; Piskorz, P.; Komaromi, I.; Martin, R. L.; Fox, D. J.; Keith, T.; Al-Laham, M. A.; Peng, C. Y.; Nanayakkara, A.; Challacombe, M.; Gill, P. M. W.; Johnson, B.; Chen, W.; Wong, M. W.; Gonzalez, C.; Pople, J. A. *Gaussian Development Version*, revision D.02; Gaussian, Inc.: Wallingford, CT, 2004.
- Becke, A. D. *J. Chem. Phys.* **1993**, *98*, 5648.
- Lee, C. T.; Yang, W. T.; Parr, R. G. *Phys. Rev. B* **1988**, *37*, 785.
- Zhang, K.; Yang, H. *J. Phys. Chem. B* **2005**, *109*, 21930.
- Kuno, M.; Fromm, D. P.; Hamann, H. F.; Gallagher, A.; Nesbitt, D. J. *J. Chem. Phys.* **2001**, *115*, 1028.
- Hou, Y. M. C.; Zhou, D.; Wang, W. *Yingyong Huaxue* **1987**, *4*, 53.
- Chang, T. L.; Cheung, H. C. *J. Phys. Chem.* **1992**, *96*, 4874.
- Dickson, R. M.; Cubitt, A. B.; Tsien, R. Y.; Moerner, W. E. *Nature* **1997**, *388*, 355.
- Nirmal, M.; Dabbousi, B. O.; Bawendi, M. G.; Macklin, J. J.; Trautman, J. K.; Harris, T. D.; Brus, L. E. *Nature* **1996**, *383*, 802.
- Tinnefeld, P.; Hofkens, J.; Hertel, D. P.; Masuo, S.; Vosch, T.; Cotlet, M.; Habuchi, S.; Mullen, K.; De Schryver, F. C.; Sauer, M. *Chem. Phys. Chem.* **2004**, *5*, 1786.
- Turro, N. J. *Modern Molecular Photochemistry*; University Science Books: Sausalito, CA, 1991.
- Mitchell, C. A.; Gurney, R. W.; Jang, S. H.; Kahr, B. *J. Am. Chem. Soc.* **1998**, *120*, 9726.
- Stefani, F. D.; Knoll, W.; Kreiter, M.; Zhong, X.; Han, M. Y. *Phys. Rev. B* **2005**, *72*, 125304.
- Verberk, R.; van Oijen, A. M.; Orrit, M. *Phys. Rev. B* **2002**, *66*, 233202.
- Kuno, M.; Fromm, D. P.; Johnson, S. T.; Gallagher, A.; Nesbitt, D. J. *Phys. Rev. B* **2003**, *67*, 125304.
- Pelton, M.; Grier, D. G.; Guyot-Sionnest, P. *Appl. Phys. Lett.* **2004**, *85*, 819.
- Hoogenboom, J. P.; den Otter, W. K.; Offerhaus, H. L. *J. Chem. Phys.* **2006**, *125*.
- Kuno, M.; Fromm, D. P.; Hamann, H. F.; Gallagher, A.; Nesbitt, D. J. *J. Chem. Phys.* **2000**, *112*, 3117.
- Maenosono, S. *Chem. Phys. Lett.* **2005**, *405*, 182.
- Kuno, M.; Fromm, D. P.; Gallagher, A.; Nesbitt, D. J.; Micic, O. I.; Nozik, A. J. *Nano Lett.* **2001**, *1*, 557.
- Nesbitt, D. J. *Abstr. Pap. Am. Chem. Soc.* **2003**, *225*, U456.
- Stratmann, R. E.; Scuseria, G. E.; Frisch, M. J. *J. Chem. Phys.* **1998**, *109*, 8218.
- McHedlov-Petrosyan, N. O.; Kukhtik, V. I.; Bezugliy, V. D. *J. Phys. Org. Chem.* **2003**, *16*, 380.
- McHedlov-Petrosyan, N. O.; Salamanova, N. V.; Vodolazkaya, N. A.; Gurina, Y. A.; Borodenko, V. I. *J. Phys. Org. Chem.* **2006**, *19*, 365.
- Jang, Y. H.; Hwang, S. G.; Chung, D. S. *Chem. Lett.* **2001**, 1316.
- Wang, X. Q.; Song, M. Y.; Long, Y. C. *J. Solid State Chem.* **2001**, *156*, 325.
- Wustholz, K. L.; Sluss, D. R. B.; Kahr, B.; Reid, P. J. Manuscript in preparation.